

Optical and electro-optical derivation of the pretransitional behavior of orientational and shear viscosities in the isotropic phase of liquid crystals

M. L. Jiménez,^{1,2} F. Mantegazza,³ L. Gallazzi,¹ G. Zanchetta,¹ and T. Bellini¹

¹*Dipartimento di Chimica, Biochimica e Biotecnologie per la Medicina, Università di Milano, 20090 Segrate (MI), Italy*

²*Department of Applied Physics, Faculty of Science, University of Granada, 18071 Granada, Spain*

³*DIMESAB, Università di Milano-Bicocca, 20052 Monza (MI), Italy*

(Received 8 March 2006; published 19 July 2006)

The pretransitional equilibrium properties of isotropic liquids in the proximity of the isotropic-nematic phase transition are well known and successfully modeled. Much less is known about the dynamic behavior, and in particular about the pretransitional viscosity. In this work we combine two techniques [dynamic light scattering (DLS) and electric birefringence spectroscopy (EBS)] offering complementary insights into both static and dynamic pretransitional behavior of the homologous *n*CB family (*n*-alkyl cyanobiphenyl). EBS explores the single molecule flipping dynamics retarded by a paranematic potential barrier and enables extracting the associated transport coefficient, which is found to be of Arrhenius type in the whole temperature range explored. DLS reflects the collective dynamics of correlated domains and depends on the viscous damping of the orientational order. Such a viscosity displays Arrhenius behavior only sufficiently far from the transition temperature, with deviations growing as a power law of the appropriate reduced temperature with exponents around 0.1.

DOI: [10.1103/PhysRevE.74.011707](https://doi.org/10.1103/PhysRevE.74.011707)

PACS number(s): 64.70.Md, 61.30.-v, 78.20.Jq

I. INTRODUCTION

The isotropic to nematic (IN) phase transition in liquid crystals (LC) is a weak first order transition where a discontinuous change of the order parameter is preceded on the high temperature side by pretransitional fluctuations of the orientational order [1,2]. As the IN transition temperature T_{NI} is approached from the isotropic phase, the correlation length for the local orientational order grows, leading to hyperbolic divergence of the susceptibilities as measured through scattered light intensity [2–8], and magnetic [5,9] and electric susceptibilities [5,10–13]. The divergences are terminated by the occurrence of the first order transition at T_{NI} , where the correlation length reaches values up to a few hundred Å [2]. Apart from minor deviations from hyperbolic behavior near the transition [3–5,8,9,14], the static properties of the IN pretransitional state are well described by the classic mean field theory proposed by Landau and deGennes [1,2], valid for temperatures that satisfy the Ginzburg criterion.

As local orientational ordering develops, its associated dynamics slows down. While the basic scaling of the pretransitional static behavior is well established [2], much less clear is the temperature dependence of viscosities and, in general, of transport coefficients of LC. Indeed, in literature examples can be found of both critical [9,15] and noncritical [3,9–11,15–19] behavior. Such findings, as far as we know, have not been clearly theoretically justified. In fact, the behavior of viscosities and transport coefficients even for the case of simple fluids is hard to model [20,21].

This paper focuses on the static and dynamic properties of the nematogenic compounds *n*CB (*n*-alkyl cyanobiphenyl) measured in the isotropic phase near the IN transition by two distinct experimental techniques, electric birefringence spectroscopy (EBS) and dynamic light scattering (DLS), providing distinct insights into the system properties. The birefringence induced in the isotropic phase by electric fields at

various frequencies comes from electric polarization and alignment of correlated domains. Accordingly, its cutoff at high frequency reflects the difficulty for each single molecule to follow the fast changes of the field and, hence, for the domain to be polarized. On the other hand, the intensity of the scattered light measures the local mean square fluctuation of the dielectric constant brought about by the fluctuations in orientational ordering. The correlation time determined by DLS is a measure of the fluctuation lifetime. Therefore, from the dynamic response of EBS and DLS we can determine the associated transport coefficients. The cutoff frequency of the electric birefringence spectra enables determining the transport coefficient associated with the single molecule dynamics. The viscosity extracted from the correlation time is instead related to the dynamics of formation of the domain. We obtain that the two transport coefficients behave differently: single molecule dynamics is hindered by a noncritical viscosity and by a paranematic potential barrier, while the transport coefficient determining the lifetime and orientational dynamics of paranematic fluctuations displays instead an unmistakable precritical character.

II. EXPERIMENTAL

A. Materials

We use LC of the family of *n*-alkyl cyanobiphenyl (Merck), whose molecules have a permanent electric dipole along the axis, two rigid phenyl rings and an alkyl chain of length *n*. Depending on this length the liquid crystal exhibits different phase behavior, as is shown in Fig. 1. Apart from the even-odd effect of the critical temperatures [1] we also observe that not all the phases are present on each liquid crystal. As the length of the flexible aliphatic chain is increased the tendency for microphase separation leading to

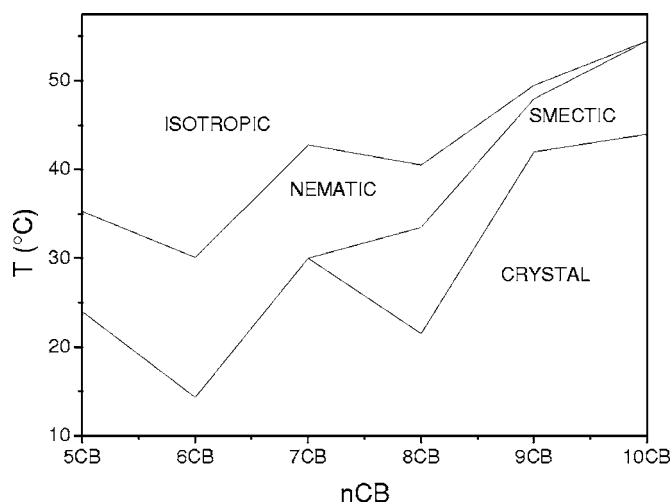


FIG. 1. Schematic Phase diagram of the nCB family.

the layered smectic structure is enhanced, while the overall molecular rigidity and hence the tendency to orientational ordering is reduced. In the case of 10CB the IN phase transition is absent and the transition from isotropic to smectic is direct.

B. The EBS experiment

In this experiment, we measure the birefringence $\Delta n = n_{\parallel} - n_{\perp}$ induced by an electric field on the isotropic phase of the LC. n_{\parallel} and n_{\perp} are, respectively, the refractive index parallel (\parallel) or perpendicular (\perp) to the electric field. The sample is kept in a cell of 200 μl of capacity that contains a pair of parallel electrodes 1 mm apart. A sinusoidal electric pulse of angular frequency ω in the range from 628×10^3 to 1900×10^6 rad/s is applied, the upper frequency limit (300 MHz) being set by inductive loops at the cell. A linearly polarized monochromatic beam emitted by a He-Ne laser source crosses the cell of optical path length of 1 cm where the electric field is perpendicular to the beam and at 45 degrees from the incident polarization. After the cell, the beam encounters (i) a quarter wave plate with fast axis parallel to the incident polarization and (ii) an analyzer at $90 - \alpha$ degrees from it, where α is a small angle enabling to enhance the signal, detect the sign of the birefringence and compensate the residual birefringence of the cell window [22]. Details about the experimental setup are described elsewhere [23].

The intensity detected after the analyzer depends on the induced birefringence. Experiments were performed in the low field “Kerr regime,” where the induced birefringence Δn is proportional to the square of the applied field, as verified in the whole frequency range explored (see Fig. 2). The Kerr constant K defined as the low field electrooptical susceptibility is

$$K = \frac{\Delta n}{\lambda E_0^2}, \quad (1)$$

where λ and E_0 are, respectively, the laser beam wavelength and the amplitude of the electric field. If we apply a sinusoidal electric pulse, the Kerr constant is composed by a dc

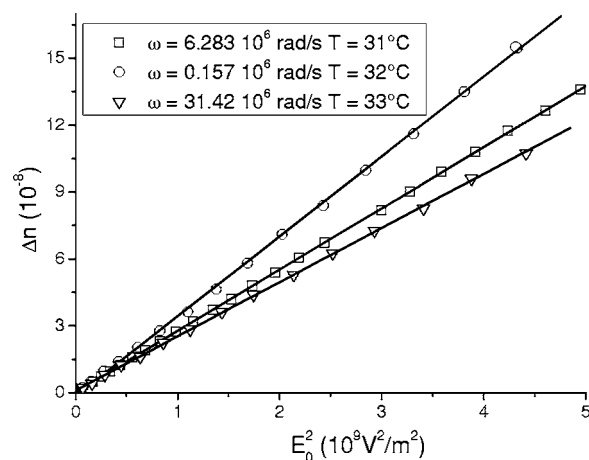


FIG. 2. Electrically induced birefringence Δn of 6CB measured at different frequencies as a function of the square of the electric field E_0 . The continuous lines show the proportionality between Δn and E_0^2 .

component K_{dc} and an ac component at frequency 2ω . In a LC, the ac component is dominated by the dynamics of the paranematic fluctuations, while the dc component is related to the amplitude of the local dielectric anisotropy at frequency ω . EBS measures the dc component of the induced birefringence as a function of the frequency of the applied electric field [22].

In Fig. 3 we present an example of the Kerr constant K_{dc} measured as a function of the frequency at four different temperatures for 5CB. All EBS spectra can be well fitted by the real part of a Debye function (lines in Fig. 3)

$$K_{dc}(\omega) = K_{\infty} + \frac{K_0 - K_{\infty}}{1 + (\omega\tau_{EB})^2}, \quad (2)$$

where K_{∞} and K_0 are, respectively, the high and low frequency asymptotic values of the Kerr constant and τ_{EB} is the inverse of the characteristic frequency of the relaxation

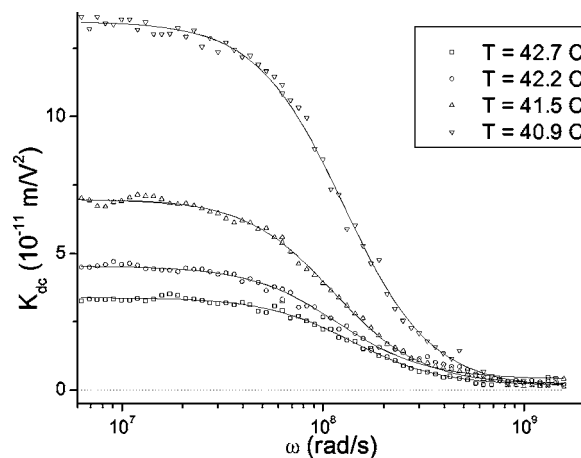


FIG. 3. DC component of the Kerr constant K_{dc} of 8CB measured as a function of the frequency ω of the external electric field at different temperatures. Lines: best fit with the Debye equation (2).

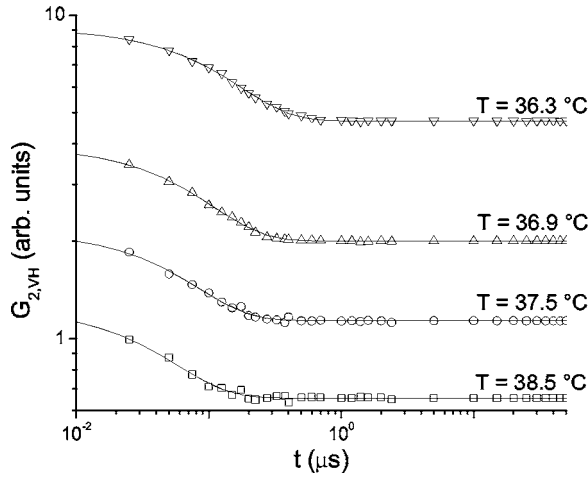


FIG. 4. Time dependence of the autocorrelation function $G_{2,VH}$ of the scattered light intensity in VH configuration of 5CB at different temperatures. Lines: best fit with a monoexponential function.

curve. Fitting Eq. (2) to the experimental spectra at different temperatures allows to obtain the temperature dependence of both the susceptibilities (K_0 and K_∞) and the dynamic response time (τ_{EB}).

Actually, in analogy with predicted dielectric spectra anomalies [24,25], deviations of Kerr spectra from the Debye-type behavior have been proposed in literature [26,27], but those departures are generally very small and not detectable within our experimental uncertainties.

C. The DLS experiment

Light scattered at 90 degrees from a He-Ne laser beam (wavelength 632.8 nm) and scattering vector $q=2.1 \times 10^7 \text{ m}^{-1}$ is collected by a single mode fiber coupling system. From the data we extract the average scattered intensity $I_{VV,VH}$ in polarized (VV) and depolarized (VH) configurations and the time autocorrelation function G_2 of the intensity of both polarized and depolarized scattered light ($G_{2,VV}$ and $G_{2,VH}$, respectively) at various temperatures. The incident beam is vertically polarized and we collect the scattered light either through a vertical polarizer (VV geometry) or through a horizontal polarizer (VH geometry). G_2 is expressed by [28]

$$G_{2,VV,VH}(t) = [\alpha g_{1(VV,VH)}^2(t) + 1] I_{VV,VH}^2, \quad (3)$$

where α is an instrumental coherence factor whose maximum value, nearly attained in single mode collection, is 1 and $g_{1(VV,VH)}$ is the normalized autocorrelation function of the scattered field. A fiber beam splitter and cross correlation enable to reliably extract correlation functions down to a retardation time of 25 ns, a limit set by the electronics of the BI9000 correlator board used in the experiment.

Within our experimental uncertainties the correlation function of the nCB liquid crystal at both VV and VH configurations is monoexponential (see Fig. 4),

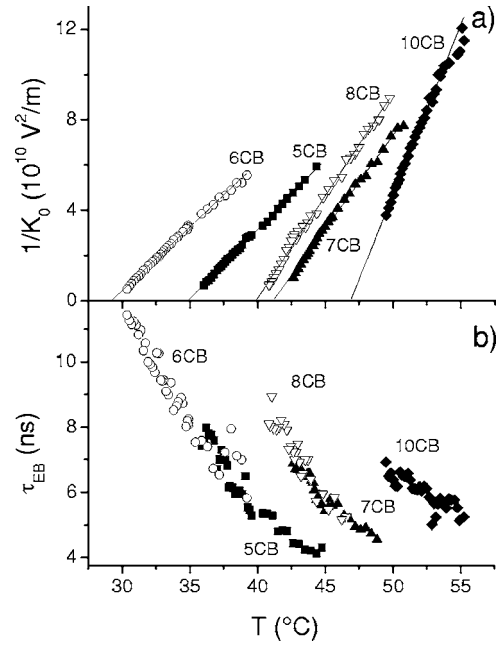


FIG. 5. (a) Inverse of the low frequency value of the birefringence $1/K_0$ and (b) characteristic times τ_{EB} measured as a function of the temperature for the nCB family. Lines: best linear fit from which the divergence temperature T_{EB}^* is obtained.

$$g_{1(VV,VH)}(t) \propto e^{-t/(2\tau_{VV,VH})}, \quad (4)$$

$\tau_{VV,VH}$ is the characteristic time of the decay in the DLS experiment in VV or VH configuration.

III. STATIC BEHAVIOR

A. Electric birefringence

In Fig. 5 the inverse of the low frequency value K_0 of the birefringence and the characteristic time τ_{EB} of the EBS spectrum are plotted as a function of the temperature for the nCB studied. The values of the Kerr constant are in line with those reported in literature [12,29]. As clearly shown in the figure, $1/K_0$ linearly depends on temperature and thus can be described by $1/K_0 \propto (T - T^*)$ where T^* is a pseudotransition temperature which would correspond to a singular point if the isotropic phase would not incur the first order IN transition. T^* is generally located about one degree below the actual transition temperature T_{NI} . This behavior is well known and can be accounted for within the frame of mean field analyses.

In the Landau-de Gennes mean field approach the free energy density F is expanded as

$$F = \frac{1}{2}As^2 - \frac{1}{3}Bs^3 + \frac{1}{4}Cs^4 + \dots, \quad (5)$$

where $s = \frac{1}{2}(3 \cos^2 \theta - 1)$ is the scalar nematic order parameter and θ is the angle between the molecular axis and the reference direction. The temperature dependence is brought into the model through $A(T) = a(T - T^*)$, where a is a constant independent of the temperature [1,2]. The first order character of the transition is ensured by a cubic term in the expansion.

TABLE I. Transition temperature T_{NI} ($^{\circ}\text{C}$), divergence temperature T^* ($^{\circ}\text{C}$) and activation energy ΔH for the $n\text{CB}$ s obtained from EBS, polarized (VV) and depolarized (VH) DLS. W is the nematic potential extracted as described in the text. $\Delta H(\eta)$, $\Delta H(\varepsilon_{\text{iso}})$, and $\Delta H(\varepsilon_{\parallel})$ are, respectively, the activation energies for the shear viscosity, for the dielectric constant in isotropic phase and for the parallel dielectric constant in the nematic phase found in literature [18,31,32]. All energy data are in kJ/mol, and their uncertainties are of the order of 15%.

$n\text{CB}$	T_{NI}	T_{EB}^*	T_{VV}^*	T_{VH}^*	ΔH_{EB}	ΔH_{VV}	ΔH_{VH}	$\Delta H(\eta)$	W	$\Delta H(\varepsilon_{\parallel})$	$\Delta H(\varepsilon_{\text{iso}})$
5	35.9	34.9	33.5	33.3	59	40	34	31	28		
6	30.4	29.2	28.9	29.0	51	41	39	32	19		
7	42.6	41.1	41.6	41.6	54	40	53	30	24	46	26
8	40.5	39.9	39.4	39.5	60	52	46	30	30	48	29
10	49.5	46.4			31			28	3		

To account for the effect of external electric fields, the Landau-de Gennes expansion is modified by adding a potential energy density W accounting for the average orientation of the permanent molecular dipole moment μ in the electric field [1],

$$W(s) = -\frac{N_A F^2 h^2 \mu^2 E_0^2}{3V k_B T} s, \quad (6)$$

where N_A is the Avogadro number, F is the reaction field factor, h is the cavity field factor, V is the molar volume, and k_B is the Boltzmann constant. In Eq. (6) we assumed the molecular permanent dipole μ to be aligned along the molecular axis and we neglected induced dipole moments. In the isotropic phase the energy is minimized by

$$s = \frac{h \varepsilon_0 \Delta \varepsilon^X E_0^2}{3a(T - T^*)}, \quad (7)$$

where ε_0 is the vacuum permittivity and $\Delta \varepsilon^X$ is the dielectric anisotropy of a perfectly aligned LC (i.e., $s=1$) given by [30]

$$\Delta \varepsilon = \varepsilon_{\parallel} - \varepsilon_{\perp} = \frac{N_A h F^2 \mu^2}{V \varepsilon_0 k_B T} s, \quad (8)$$

$$\Delta \varepsilon^X = \Delta \varepsilon(s=1), \quad (9)$$

$\varepsilon_{\parallel, \perp}$ is the dielectric constant when the electric field is applied parallel or perpendicular to the nematic director. Since the birefringence Δn is proportional to s [23]:

$$\Delta n = \Delta n^X \left\langle \frac{3 \cos^2 \theta - 1}{2} \right\rangle = \Delta n^X s, \quad (10)$$

where Δn^X is the birefringence of a perfectly aligned LC, we can combine equations and obtain

$$\Delta n = \frac{h E_0^2 \Delta n^X \varepsilon_0 \Delta \varepsilon^X}{3a(T - T^*)}. \quad (11)$$

In Table I we present T_{NI} and T_{EB}^* as obtained from the fitting of the data in Fig. 5(a) with Eq. (11). The transition temperatures are in agreement with that found in literature, including the already well documented even-odd effect [1].

The pretransitional behavior of K_0 can be intuitively understood as follows. The electric field coupling of the single

molecules is always smaller than the molecular field that keeps the orientational order. Hence, the only effect of the electric field is the flipping of the molecule that does not oppose the molecular field. The torque added up for all the molecules inside the correlated domain becomes large enough to induce an orientation of the whole domain along the field, leading to an enhanced electro-optical susceptibility. Far from the transition, the domains are very small and thermal agitation hinders the orientation, hence there is not an observable birefringence. As temperature decreases, the domains become larger and hence their ability to orient, yielding to an increase of the birefringence. The divergence of the birefringence goes in parallel with the divergence of the correlation length.

The K_{∞} data range between 10^{-12} and 10^{-11} m/V² are in agreement with those previously reported [33], and despite they are very noisy, have a decreasing tendency with temperature. $K_0/K_{\infty} \approx 30 \pm 10$, which roughly agrees with the value $\frac{\varepsilon_{\parallel} - \varepsilon_{\perp}}{n_{\parallel}^2 - n_{\perp}^2} \approx 20$ extracted from literature values [34].

The transition from isotropic to smectic 10CB takes place at 3.6 degrees higher than the divergence temperature T^* (while in the other cases the difference was around 1 degree). That means that the correlation length before the transition is much smaller than in the other $n\text{CB}$ studied and hence the Kerr constant values K_0 are smaller than the data of the other $n\text{CB}$ studied.

B. Scattered light

In Fig. 6 we plot the ratio of the temperature and scattered intensity (I_{VV} and I_{VH}) obtained by fitting Eq. (4) to the data of the correlation function $G_2(t)$ in the VV and VH configurations, respectively. Analogously to what was found with the Kerr constant, $T/I_{\text{VV}, \text{VH}}$ depends linearly on T , vanishing at an extrapolated T_{VV}^* and T_{VH}^* whose values closely match those found from the EBS experiment (see Table I).

The intensity scattered in the isotropic phase by a LC in the proximity of T_{NI} depends on the magnitude and size of local fluctuation of the dielectric constants, and thus light scattering is the most direct technique to detect the growth of the short-ranged orientational order. As we approach the critical temperature, the correlation length increases and thus the intensity of the scattered light. An explanation of this

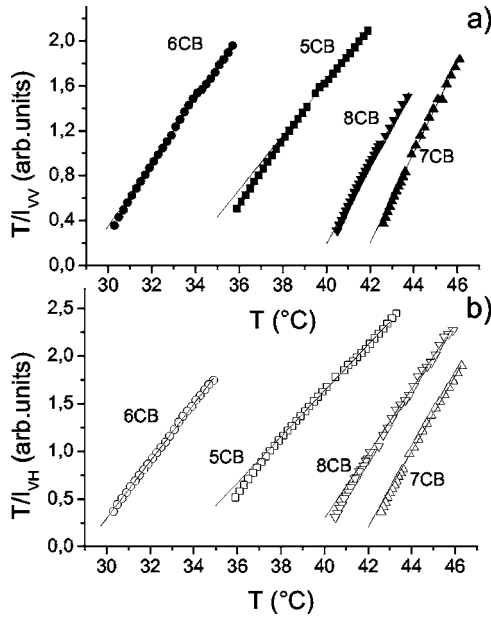


FIG. 6. (a) Ratio of the temperature and the intensity of the scattered light (a) T/I_{VV} and (b) T/I_{VH} measured as a function of the temperature. The lines represent the best linear fit to the high temperature data.

phenomenon can be found in the frame of the Landau-de Gennes model [35]. Using the Gaussian approximation [that is, considering only the s^2 term in Eq. (5)] it is obtained that in VV and VH configurations, the scattered intensities are, respectively [35],

$$I_{VV} \propto \frac{k_B T}{a(T - T^*)},$$

$$I_{VH} = \frac{3}{4} I_{VV}. \quad (12)$$

Hence, a plot of $T/I_{VV,VH}$ should scale linearly with $T - T^*$ as shown in Fig. 6.

If we observe carefully the static results at temperatures just above the transition, it can be seen that the light scattering intensity deviates from the $(T - T^*)^{-1}$ behavior. These deviations have been already studied [3–5] and justified since near the transition the fluctuation becomes important and the associated free energy expansion, from which the probability of the fluctuation is calculated, cannot be cut at the second order term. It has been also shown that including cubic and quartic terms is enough to account for the whole experimental set of data of the susceptibilities [3–5]. Actually, according to our measurements, such deviations are certainly present, but are smaller than those found in literature. At the contrary, in EBS measurements the deviations, if present, are very small and not appreciable given our experimental uncertainties.

Because of the short correlation lengths of 10CB, the combination of weak scattering intensities and short correlation times makes impossible to perform DLS measurements on this compound.

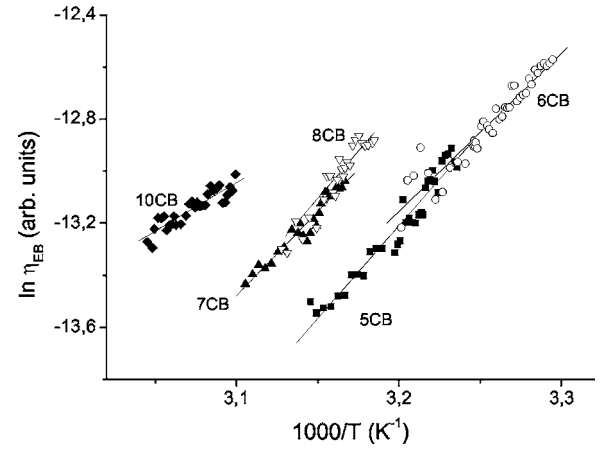


FIG. 7. Arrhenius plot of the viscosity η_{EB} extracted from EBS data for the nCB family studied. Line: linear fit curves.

IV. DYNAMIC BEHAVIOR

A. Shear viscosity from EBS

The measured characteristic times τ_{EB} [see Fig. 5(b)] are of the same order than those found in literature [29,33], but precision of our measurements permits, for the first time, to determine its temperature dependence. We observe that τ_{EB} increases but it does not diverge approaching the transition temperature and so no evidence of critical slowing down is shown. τ_{EB} displays remarkable pairing of 5CB and 6CB data, and of 7CB and 8CB data, possibly reminiscent of the standard odd-even effect.

As the frequency of the electric field increases, the ability of the molecules to orient along the field decreases, in turn yielding a decreased Δn_{dc} . Therefore, the characteristic time τ_{EB} is related to the flipping time necessary to orient the permanent dipole of the molecule along the external electric field.

In a very first approximation, neglecting the molecular fields effects, we can apply the Debye friction model for the orientation relaxation time of spheres [36]:

$$\frac{1}{\tau_{EB}} \propto \frac{k_B T}{\eta_{EB}}, \quad (13)$$

where η_{EB} is the viscosity extracted from EBS. Accordingly, in this simplified view, η_{EB} is obtained by the following proportionality relation:

$$\eta_{EB} \propto \tau_{EB} T. \quad (14)$$

Quite generally, viscosities exhibit activated dynamics behavior as described by the following Arrhenius equation

$$\eta = \eta_0 \exp(\Delta H/k_B T), \quad (15)$$

where η_0 is independent of the temperature and ΔH is the activation energy. In analogy, we can represent our η_{EB} data in the Arrhenius plot as in Fig. 7. The linearity in the data indicates that the molecular flipping in the pretransitional regime is an activated process, whose activation energy ΔH_{EB} is given in Table I.

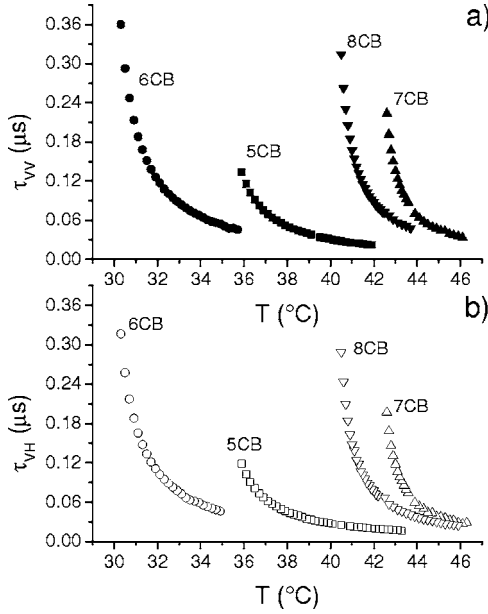


FIG. 8. Characteristic time (a) τ_{VV} and (b) τ_{VH} measured as a function of the temperature for the n CBs studied.

As evident by inspecting the data in Table I, ΔH_{EB} is systematically larger than the activation energies obtained through other experimental techniques such as rheology, dielectric spectroscopy and DLS.

B. Orientational viscosity from DLS

1. Role of viscosity in the DLS

Figure 8 shows the characteristic time $\tau_{VV,VH}$ of the correlation function $G_2(t)$. Experimentally, the values are around one order of magnitude larger than τ_{EB} in agreement with a supramolecular dynamics. The values of the characteristic time τ_{VH} are very similar to those found in Refs. [15,19], where the rate Γ of the fluctuations is obtained from light scattering spectra.

The equation of motion for the orientational order parameter can be described by the Onsager relations for the coupled flows of the tensorial order parameter $Q_{\alpha\beta}$ and the shear rate $v_{\alpha\beta}$,

$$Q_{\alpha\beta} = \varepsilon_{\alpha\beta} - \frac{1}{3} \varepsilon_{\gamma\gamma} \delta_{\alpha\beta}, \quad (16)$$

$$v_{\alpha\beta}(\vec{r}, t) = \frac{1}{2} \left(\frac{\partial v_\alpha(\vec{r}, t)}{\partial x_\beta} + \frac{\partial v_\beta(\vec{r}, t)}{\partial x_\alpha} \right) \quad (17)$$

being $\varepsilon_{\alpha\beta}$ the elements of the dielectric tensor, $\delta_{\alpha\beta}$ the Dirac delta, v_α the α component of the velocity and x_α the α Cartesian coordinate. The Onsager relations for such coupled hydrodynamic flows are [35]

$$\sigma_{\alpha\beta}(\vec{r}, t) = \eta v_{\alpha\beta}(\vec{r}, t) + 2\mu \dot{Q}_{\alpha\beta}(\vec{r}, t), \quad (18)$$

$$\Phi_{\alpha\beta}(\vec{r}, t) = \mu v_{\alpha\beta}(\vec{r}, t) + \nu \dot{Q}_{\alpha\beta}(\vec{r}, t), \quad (19)$$

where $\sigma_{\alpha\beta}(\vec{r}, t)$ is the $\alpha\beta$ component of the hydrodynamic stress tensor and $\Phi_{\alpha\beta}(\vec{r}, t) = -A Q_{\alpha\beta}(\vec{r}, t)$ is the force conjugate to the order parameter. η is the shear viscosity, μ is the transport coefficient associated to the momentum transfer between collective rotation and translation, and ν is the transport coefficient characterizing the dissipation of the order parameter fluctuations (orientational viscosity). ν express the fast collision that lead to a slow decay of the order parameter fluctuation in a purely dissipative process.

In the VV configuration, the scattered light measures the mean square fluctuations that are not coupled to the shear fluxes [$\langle Q_{yy}^2(q, \omega) \rangle$] if we set the wave number $\hat{z} \parallel \vec{q}$] and the intensity spectrum has a Lorentzian shape,

$$I_{VV}(q, \omega) \propto \langle Q_{yy}^2(q, \omega) \rangle = \langle Q_{yy}^2(q, 0) \rangle \frac{2\Gamma}{\Gamma^2 + \omega^2}, \quad (20)$$

where the ‘‘Litster width’’ Γ [9] is given by

$$\Gamma = A(T)/\nu = a(T - T^*)/\nu. \quad (21)$$

In the VH configuration,

$$I_{VH} \propto \langle Q_{yy}^2(q, \omega) \rangle \sin^2 \frac{\phi}{2} + \langle Q_{yz}^2(q, \omega) \rangle \cos^2 \frac{\phi}{2}, \quad (22)$$

where ϕ is the scattering angle. The coupling between the shear rate and the order fluctuations leads to the second addend in Eq. (22). It has the shape:

$$\begin{aligned} \langle Q_{yz}^2(q, \omega) \rangle &= \frac{\langle Q_{yz}^2(q, 0) \rangle (\omega^2 + bcq^4)}{(\omega^2 - \Gamma bq^2)^2 + \omega^2 (\Gamma + cq^2)^2} \\ &= \langle Q_{yz}^2(q, 0) \rangle \left(\frac{M_1 \Gamma_1}{\omega^2 + \Gamma_1^2} - \frac{M_2 \Gamma_2}{\omega^2 + \Gamma_2^2} \right), \end{aligned} \quad (23)$$

where $b = \eta/\rho$, $c = b(1 - 2\mu^2/\nu\eta)$, ρ is the mass density, $M_1 \approx b/c$, $M_2 \approx b/c - 1$, $\Gamma_1 \approx \Gamma b/c$, and $\Gamma_2 \approx cq^2$.

Hence, in the VV configuration the normalized autocorrelation function of the scattered field g_{1VV} in the time domain is well described by a monoexponential decay,

$$g_{1,VV}(q, t) \propto e^{-\Gamma t} \quad (24)$$

while in the VH case we expect

$$g_{1,VH}(q, t) \propto \xi_0 e^{-\Gamma t} + \xi_1 (M_1 e^{-\Gamma_1 t} - M_2 e^{-\Gamma_2 t}), \quad (25)$$

where ξ_0 and ξ_1 are normalization constants. The observation of more than one exponential function (or Lorentzian function in the frequency domain) is not possible in our experimental conditions, as $\Gamma_1 \approx \Gamma$ and the third addend in Eq. (25) decays too fast to be observed. Hence we force the simplification

$$g_{1,VH}(q, t) \approx e^{-\Gamma' t} \quad (26)$$

where Γ' is some average value between Γ and Γ_1 . In the VH configuration we obtain a systematically smaller value for all n CB at all temperature of the characteristic time ($\tau_{VV}/\tau_{VH} \approx 1.14 \pm 0.04$), from which we can estimate ($\Gamma' \approx \frac{\Gamma + \Gamma_1}{2}$) that

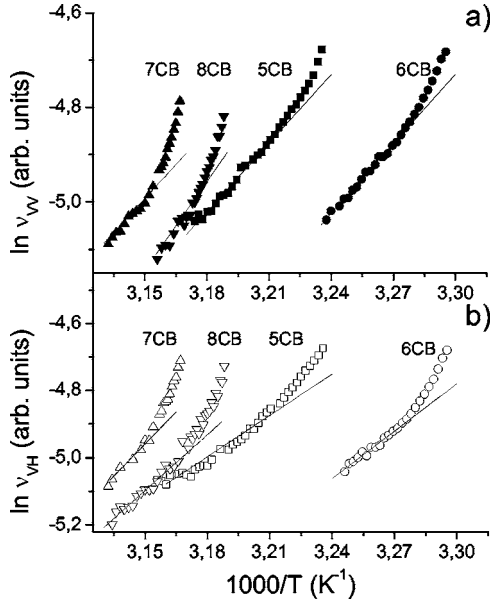


FIG. 9. Arrhenius plot of the orientational viscosities ν_{VV} and ν_{VH} as obtained from DLS experiments in both (a) VV and (b) VH configurations. Lines correspond to the high temperature Arrhenius law.

$2\mu^2/\nu\eta \approx 0.22 \pm 0.04$, similar to the values reported in the literature [9,15].

2. Experimental values of the orientational viscosity

Comparing Eq. (4) with Eqs. (24) and (26) one can derive a relation between the decay time $\tau_{VV,VH}$ and the orientational viscosity $\nu_{VV,VH}$

$$\tau_{VV,VH} = \frac{\nu_{VV,VH}}{2a(T - T^*)}, \quad (27)$$

where $\nu_{VV} = \nu$ and $\nu_{VH} \approx \nu$. Hence, we can extract the orientational viscosity $\nu_{VV,VH}$ from the measured values of the time decay in the DLS (VV and VH) experiment. Namely, from Eq. (12) and Eq. (21) it is straightforward to see that

$$\nu_{VV,VH} \propto \frac{T\tau_{VV,VH}}{I_{VV,VH}}. \quad (28)$$

In this way $\nu_{VV,VH}$ is extracted combining static and dynamic light scattering data, which were simultaneously taken in each experimental condition. This is why we prefer to extract $I_{VV,VH}$ directly from G_2 rather than through the more standard procedure of averaging of multiple speckle detection.

The viscosity ν_{VV} and ν_{VH} extracted from DLS measurements are shown in an Arrhenius plot in Fig. 9. Clearly, the viscosity deviates from Arrhenius behavior near to the transition. Note that such divergence occurs for every nCB and hence cannot be due to the small deviations of the scattered intensity from the mean field hyperbolic behavior (see Fig. 6), which is not always observed. This is the case of 6CB (VH), where the deviation from linearity of T/I_{VH} is nearly absent. Indeed, if we substitute $T/I_{VV,VH}$ in Eq. (28) by the linear fitting in Fig. 6, the divergence would still be there.

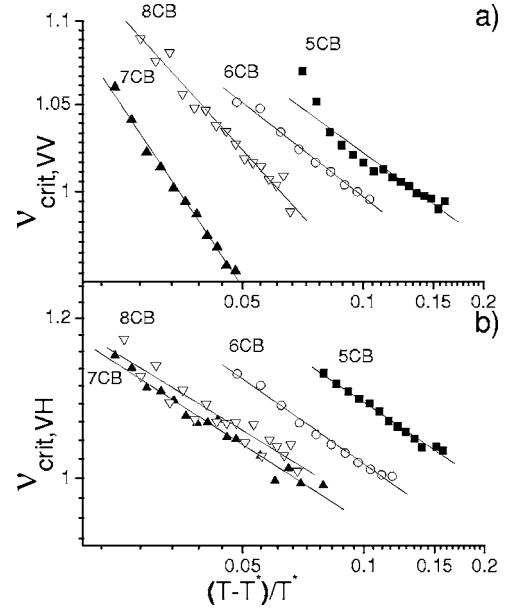


FIG. 10. Critical viscosity $\nu_{crit\,VV,VH}$ as a function of the reduced temperature $\frac{T-T^*}{T^*}$ extracted from the low temperature DLS data of Fig. 9. (a) Data from VV and (b) data from VH experiments. Lines correspond to a power law with the exponent $z_\eta \approx 0.1$.

We can express the viscosities in Fig. 9 as a product of a noncritical Arrhenius viscosity $\nu_{Arr\,VV,VH}$ and a critical viscosity $\nu_{crit\,VV,VH}$,

$$\nu_{VV,VH} = \nu_{crit\,VV,VH}(T)\nu_{Arr\,VV,VH}(T). \quad (29)$$

As a consequence, the activation energy (ΔH_{VV} , ΔH_{VH}) for each nCB (see Table I) can be extracted only from the high temperature data, by fitting with an Arrhenius law.

Figure 10 represents $\nu_{crit\,VV,VH}$ as a function of the reduced temperature $\epsilon = \frac{T-T^*}{T^*}$ in a double logarithmic scale near T^* , where T^* has been taken in every case from the DLS data in Table I. Although the data range is too narrow to extract reliable critical exponents, it can be seen that the equation $\nu_{crit\,VV,VH} \propto \epsilon^{-z_\eta}$ describes reasonably well the critical viscosity with a critical exponent z_η ranging from 0.08 to 0.15 for both the VV and VH configuration and for all the LC studied.

V. DISCUSSION

A. Characteristic times and activation energies of EBS

It is interesting to compare our EBS data with the dielectric spectra found in literature, since both quantities are related to the polarizability of the system and in both cases the observed dynamics reflects the single molecule kinetics. We already noticed in commenting Table I that the activation energies of EBS are larger than those extracted from DLS and those reported in literature for viscosity and dielectric constant. We show here that this anomaly of ΔH_{EB} combines with other intriguing differences between EBS and dielectric spectroscopy, suggesting fundamental differences between the two experiments.

In Fig. 11 we overplot our EBS data and dielectric data taken from Bose *et al.*, Ref. [31], for 8CB. Although data are

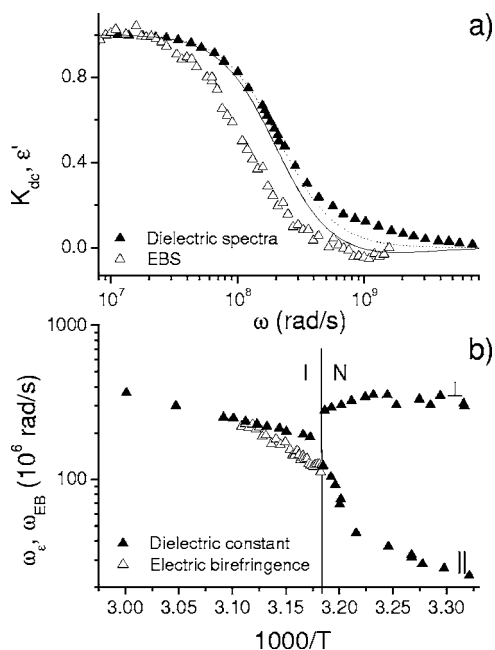


FIG. 11. (a) Normalized dielectric constant ϵ' (data from Ref. [31]) and normalized Kerr constant K_{dc} for 8CB at 41.5 C. Dashed line is the best Debye fitting curve to the dielectric spectra. Solid line is the prediction of the droplet model for the Kerr constant. (b) Arrhenius plot of the characteristic frequency of the dielectric relaxation (ω_c , full symbols) in the isotropic and nematic phases (data from Ref. [31]) and of EBS relaxation ($\omega_{EB} = 1/\tau_{EB}$, open symbols, data from Fig. 5). Data taken for 8CB.

overall similar, differences are evident. The normalized dielectric spectrum ϵ' exhibits more than one characteristic time, as it is shown by the deviation from the Debye curve [dotted line in Fig. 11(a)] at high frequency, while the normalized Kerr constant K_{dc} decays through a single relaxation process (see Fig. 3). Also, EBS dynamics is systematically slower and with an unmistakably larger activation energy.

It is worth to note that dielectric spectrum displayed in Fig. 11(a) is just one example in the many offered by the wide body of literature [17,32,37–44], all sharing non-Debye behavior and characteristic frequency larger than our Kerr measurements, besides some slight quantitative differences.

To picture the effect of paranematic fluctuations in EBS and dielectric spectroscopy, and possibly spot their intrinsic differences, it is useful to pursue the simple description of fluctuations as given by the so-called droplet model of critical phenomena [45]. Accordingly, we envision the pretransitional LC as an ensemble of nematic droplets, each described as if suspended in the isotropic phase. The order parameter is assumed to be the same within every droplet while the droplet directors are taken to be independent from each other. The dielectric anisotropy of each droplet is characterized by $\epsilon_{\parallel,D}$ and $\epsilon_{\perp,D}$ together with the respective relaxation frequencies $\omega_{\parallel,D}$ and $\omega_{\perp,D}$. The angular distribution of the droplets follows the Boltzmann function $f(\theta) \approx e^{-V_d(\theta)/k_B T}$, where V_d is the electric energy of the droplet in the external electric field and θ is the angle between the director of the droplet and the electric field. The total dielectric constant of the dispersion is proportional to the average value of the dipole moment of

the droplets. On the other hand, the electric birefringence of the whole system is given by the average value of $[3 \cos^2(\theta) - 1]/2$. On the basis of this model, one can characterize both the dielectric and the Kerr constants with the same set of parameters. By fitting the dielectric spectra to a double Debye, we extracted $\epsilon_{\parallel,D}$, $\epsilon_{\perp,D}$, $\omega_{\parallel,D}$, and $\omega_{\perp,D}$, from which we constructed the expected behavior of the Kerr constant [solid line in Fig. 11(a)]. In spite of the fact that the experimental Debye shape of the Kerr constant is approximately reproduced, the large difference between the dielectric and Kerr characteristic frequencies observed in Fig. 11(b) cannot be explained by this standard form of the droplet model.

A clue of how the paranematic state could be better portrayed to allow for the observed EBS behavior, is given by the intriguing matching of the EBS characteristic frequency and activation energy in the isotropic phase with those of the parallel dielectric constant in the nematic phase [see Fig. 11(b) and Table I]. It is thus quite tempting to quantify the difference in activation energies by introducing into the EBS analysis the nematic retardation factor g , a measure of the potential barrier W given by nematic molecular arrangement [46]. Accordingly, $\Delta H_{EB} = W + \Delta H_{\eta}$, enabling us to use the activation energy of the shear viscosity reported in literature [18] to obtain the estimate of W reported in Table I. We obtain rather large values for W .

All these observations would coherently add up in a modified droplet model, where the droplet's order parameter S_D is not the same in every droplet, but rather follows a statistical distribution. This assumption would intrinsically yield relevant differences between EBS and dielectric spectroscopy, since droplets would contribute to the Kerr constant proportionally to S_D^2 while their contribution to the dielectric constant is basically independent from S_D . Such a weighting factor makes EBS dominated by the most ordered, and thus dynamically slowest, paranematic correlated domains. In this sense, and despite the paradoxical quality of the sentence, EBS is a tool to measure the nematic properties of the isotropic phase.

B. Critical behavior of ν

The only precedent results about the divergence of the orientational viscosity refer to c [Eq. (23)], which was measured for MBBA (MethoxyBenzylidene ButylAniline), where a qualitatively pretransitional enhancement is noticed [9], and for 6CB, where a critical exponent 0.15 has been obtained by using an optical beating spectroscopy technique whose spectra are mainly governed by the second addend in Eq. (22) [15]. More extended studies have been devoted to simple fluids, where the critical behavior of the different transport coefficients has been reported [21]. For example, near the gas-liquid transition the shear viscosity and the thermal conductivity present a weak pretransitional behavior (critical exponents $x_{\eta} = 0.041$ and $x_{\lambda} = 0.6$, respectively [47]). In this context, the small values of the critical exponent we find (z_{η} between 0.08 and 0.14) are in reasonable agreement with those found in the literature [15,21,48,49].

As far as we know, there is no theoretical frame for the dynamics of the pretransitional paranematic behavior. Hence,

we can only make some analogies with the existing models. The dynamics analyzed in simple fluids is described by different models, and renormalization group calculations can lead to different dynamic critical exponents. In fact, the dynamic critical exponents depend on the type of stochastic equation for the order parameter fluctuations. For example, the gas-liquid transition is described by the model H [20,21]. In contrast, the most appropriate to our case is model A, valid for purely dissipative dynamics of a nonconserved order parameter. However, this model is suitable for second order transitions, as the renormalization calculations are based on the thermodynamic force obtained from the Ginzburg-Landau-Wilson Hamiltonian, which is formally different from the Landau-de Gennes expansion. In fact, the theoretical value $z_\eta=0.44$ is far from what we find.

VI. CONCLUSIONS

We have shown that EBS and DLS techniques enable to obtain two different transport coefficients. With EBS we access the dynamics of a single molecule orientation inside the pretransitional domain. On the other hand, with DLS we access the dynamics of the order parameter fluctuation. The two transport coefficients present different qualitative and quantitative behavior. The viscosity obtained from EBS follows an Arrhenius law with activation energies larger than those of the shear viscosity and dielectric characteristic times. In DLS, the viscosity data display activated dynamics

only far from the transition, with activation energies similar to those reported for the shear viscosity of the isotropic phase. Near the transition, instead, the viscosity obtained from DLS shows a clear pretransitional behavior with small critical exponents. A theoretical description accounting for the critical-like observed behavior is still missing.

The differences of EBS data with respect to dielectric spectra suggest that these methods assess different features of the pretransitional system despite the similarities between the two techniques. This is because dielectric measurements reflect an unbiased average on local molecular environments, while the Kerr coefficient gathers larger contributions from the more correlated region, which also contribute with the slowest dynamics. This is apparent from a combination of features of EBS spectra in the isotropic phase of LC, approximating corresponding features observed in the nematic phase: (i) the frequency dependence is well represented by a Debye relaxation, (ii) the activation energy is similar to the activation energy of the parallel dielectric constant of nematics, and (iii) the characteristic frequency matches that of the parallel dielectric constant of nematics. EBS thus appears as a tool offering insights into the local orientational ordering of molecular fluids.

ACKNOWLEDGMENTS

The authors wish to thank G. Iannacchione and W. H. de Jeu for the useful discussions. This work was partially supported by CNR-INFM.

-
- [1] S. Chandrasekhar, *Liquid Crystals* (Cambridge University, Cambridge, 1977).
 - [2] P. G. de Gennes and J. Prost, *The Physics of Liquid Crystals* (Clarendon, Oxford, 1993).
 - [3] T. W. Stinson and J. D. Litster, *Phys. Rev. Lett.* **25**, 503 (1970).
 - [4] H. Zink and W. H. de Jeu, *Mol. Cryst. Liq. Cryst.* **124**, 287 (1985).
 - [5] E. F. Gramsbergen, L. Longa, and W. H. de Jeu, *Phys. Rep.* **135**, 195 (1986).
 - [6] J. P. McClymer and P. H. Keyes, *Phys. Rev. A* **42**, 4764 (1990).
 - [7] L. M. Blinov and V. G. Chigrinov, *Electrooptic Effects in Liquid Crystals Materials* (Springer, New York, 1994).
 - [8] J. Fuchs and W. Burchard, *J. Phys. II* **4**, 1451 (1994).
 - [9] T. W. Stinson, J. D. Litster, and N. A. Clark, *J. Phys. (Paris), Colloq.* **33**, 69 (1972).
 - [10] M. Schadt, *J. Chem. Phys.* **67**, 210 (1977).
 - [11] H. J. Coles, *Chem. Phys. Lett.* **59**, 168 (1978).
 - [12] E. I. Ryumtsev, T. A. Rotinyan, and V. N. Tsvetkov, *Sov. Phys. Dokl.* **25**, 837 (1980).
 - [13] L. Schenider and J. H. Wendorff, *Liq. Cryst.* **22**, 29 (1997).
 - [14] M. A. Anisimov, *Critical Phenomena in Liquids and Liquid Crystals* (Gordon and Breach, Amsterdam, 1991).
 - [15] T. Ueno, K. Sakai, and K. Takagi, *Phys. Rev. E* **54**, 6457 (1996).
 - [16] G. K. L. Wong and Y. R. Shen, *Phys. Rev. A* **10**, 1277 (1974).
 - [17] M. Ginovska, G. Czechowski, A. Andonovski, and J. Jazdyn, *Pol. J. Chem.* **75**, 1505 (2001).
 - [18] J. Jazdyn, G. Czechowski, and T. Lech, *Acta Phys. Pol. A* **101**, 495 (2002).
 - [19] S. Takagi and H. Tanaka, *Phys. Rev. Lett.* **93**, 257802 (2004).
 - [20] P. C. Hohenberg and B. I. Halperin, *Rev. Mod. Phys.* **49**, 435 (1977).
 - [21] A. Onuki, *Phase Transition Dynamics* (Cambridge University Press, Cambridge, 2002).
 - [22] F. Mantegazza, T. Bellini, M. Buscaglia, V. Degiorgio, and D. A. Saville, *J. Chem. Phys.* **113**, 6984 (2000).
 - [23] E. Fredericq and C. Houssier, *Electric Dichroism and Electric Birefringence* (Clarendon, Oxford, 1973).
 - [24] W. T. Coffey, Yu. P. Kalmykov, and S. V. Titov, *J. Chem. Phys.* **116**, 6422 (2002).
 - [25] J. L. Déjardin, *Phys. Rev. E* **68**, 031108 (2003).
 - [26] W. T. Coffey, D. S. F. Crothers, Y. P. Kalmykov, and P. M. Déjardin, *Phys. Rev. E* **71**, 062102 (2005).
 - [27] J. L. Déjardin and J. Jazdyn, *J. Chem. Phys.* **122**, 074502 (2005).
 - [28] R. Pecora, *Dynamic Light Scattering. Applications of Photon Correlation Spectroscopy* (Plenum, New York, 1985).
 - [29] E. I. Ryumtsev, M. A. Agafonov, R. A. Rotinyan, and V. N. Tsvetkov, *Sov. Phys. Dokl.* **29**, 1040 (1984).
 - [30] J. Thoen and T. K. Bose, in *Handbook of Low and High Di-*

- electric Constant Materials and Their Application*, edited by H. S. Nalwa (Academic, New York, 1999).
- [31] T. K. Bose, R. Chahine, M. Merabet, and J. Thoen, *J. Phys. (Paris)* **45**, 1329 (1984).
- [32] T. K. Bose, B. Campbell, S. Yagihara, and J. Thoen, *Phys. Rev. A* **36**, 5767 (1987).
- [33] M. Caggioni, A. Giacometti, T. Bellini, N. A. Clark, F. Mantegazza, and A. Maritan, *J. Chem. Phys.* **122**, 214721 (2005).
- [34] S. Elston and R. Sambles, *The Optics of Thermotropic Liquid Crystals* (Taylor and Francis, London, 1998).
- [35] P. G. de Gennes, *Mol. Cryst. Liq. Cryst.* **12**, 193 (1971).
- [36] C. J. F. Böttcher and P. Bordewijk, *Theory of Electric Polarization II. Dielectrics in Time-Dependent Fields* (Elsevier, Amsterdam, 1978).
- [37] J. M. Wacrenier, C. Druon, and D. Lippens, *Mol. Phys.* **43**, 97 (1981).
- [38] A. Hourri, P. Jamée, T. K. Bose, and J. Thoen, *Liq. Cryst.* **29**, 459 (2002).
- [39] B. A. Belyaev, N. A. Drokin, V. F. Shabanov, and V. N. Shepov, *Phys. Solid State* **45**, 598 (2003).
- [40] J. Jadzyn, G. Czechowski, C. Legrand, and R. Douali, *Phys. Rev. E* **67**, 041705 (2003).
- [41] J. Czub, U. Gubernat, B. Gestblom, R. Dabrowski, and S. Urban, *Z. Naturforsch., A: Phys. Sci.* **59**, 316 (2004).
- [42] J. Jadzyn, G. Czechowski, J. L. Dejardin, and M. Ginovska, *J. Phys.: Condens. Matter* **17**, 813 (2005).
- [43] G. Sinha, J. Leys, C. Glorieux, and J. Thoen, *Phys. Rev. E* **72**, 051710 (2005).
- [44] B. A. Belyaev, N. A. Drokin, and V. F. Shabanov, *Phys. Solid State* **48**, 993 (2006).
- [45] M. E. Fisher, in *Critical Phenomena*, Proceedings of the International School of Physics Summer School, Enrico Fermi, Course LI, Varena, 1970, edited by M. S. Green (Academic, New York, 1971).
- [46] W. H. de Jeu, in *Liquid Crystals, Solid State Physics: Advances in Research and Applications, Supplement 14*, edited by L. Liebert (Academic, New York, 1978).
- [47] J. V. Sengers and P. H. Keyes, *Phys. Rev. Lett.* **26**, 70 (1971).
- [48] R. Behrends and U. Kaatze, *Phys. Rev. E* **68**, 011205 (2003).
- [49] I. Iwanowski, R. Behrends, and U. Kaatze, *J. Chem. Phys.* **120**, 9192 (2004).